THE JOURNAL OF PHYSICAL CHEMISTRY C
A JOURNAL OF THE AMERICAN CHEMICAL SOCIETY

pubs.acs.org/JPCC

Article

Design Principles for the Development of Gd(III) Polarizing Agents for Magic Angle Spinning Dynamic Nuclear Polarization

Yu Rao, Chad T. Palumbo, Amrit Venkatesh, Megan Keener, Gabriele Stevanato, Anne-Sophie Chauvin, Georges Menzildjian, Sergei Kuzin, Maxim Yulikov, Gunnar Jeschke, Anne Lesage, Marinella Mazzanti, and Lyndon Emsley*

Cite This: *J. Phys. Chem. C* 2022, 126, 11310–11317

Read Online

ACCESS | Metrics & More | Article Recommendations | Supporting Information

ABSTRACT: Nuclear magnetic resonance suffers from an intrinsically low sensitivity, which can be overcome by dynamic nuclear polarization (DNP). Gd(III) complexes are attractive exogenous polarizing agents for magic angle spinning (MAS) DNP due to their high chemical stability in contrast to nitroxide-based radicals. However, even the state-of-the-art Gd(III) complexes have so far provided relatively low DNP signal enhancements of ca. 36 in comparison to standard DNP biradicals, which show enhancements of over 200. Here, we report a series of new Gd(III) complexes for DNP and show that the observed DNP enhancements of the new and existing Gd(III) complexes are inversely proportional to the square of the zero-field splitting (ZFS) parameter *D*, which is in turn determined by the ligand-type and the local coordination environment. The experimental DNP enhancements at 9.4 T and the ZFS parameters measured with pulsed electron paramagnetic resonance (EPR) spectroscopy agree with the above model, paving the way for the development of more efficient Gd(III) polarizing agents.

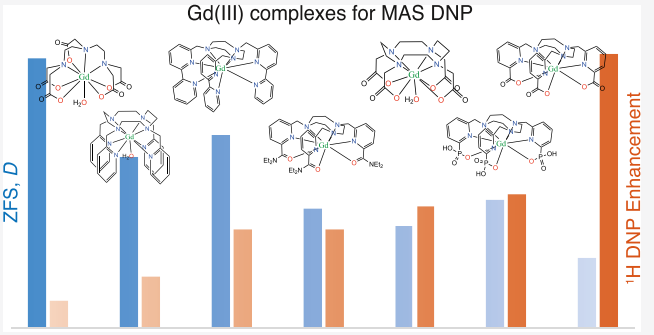

INTRODUCTION

Solid-state NMR is a well-developed characterization technique to probe atomic-level structure and dynamics in solids.[1,2] However, the application of NMR is frequently limited by its low intrinsic sensitivity primarily due to the small population difference between nuclear spin states. Dynamic nuclear polarization (DNP) improves the sensitivity of NMR by transferring the high polarization of electron spins to nuclear spins; this is routinely achieved by saturating the EPR transitions of a polarizing agent at low temperatures (100 K) using high-power microwaves.[3−5] Typically, the abundant ^{1}H spins are hyperpolarized, and the resulting hyperpolarization is transferred to other heteronuclei such as ^{13}C, ^{15}N, ^{29}Si, etc. Aided by advances in the rational design of polarizing agents and commercial instrumentation, DNP is now routinely applied to accelerate NMR experiments with biomolecules, materials, and surfaces by several orders of magnitude.[2,4,6−12]

MAS DNP samples are typically prepared by impregnating the target solid with a solution of nitroxide-based biradicals such as TEKPol,[13] AMUPol,[14] AsymPolPOK,[15] TinyPol,[16] and HydrOPol.[17] Recently, hybrid BDPA/trityl nitroxide biradicals[18,19] have been proposed for high-field (800 MHz and above) DNP experiments. However, nitroxide-based polarizing agents may react with sensitive samples such as catalysts and surfaces of materials that contain active species. Furthermore, nitroxide radicals are unstable, for example, in reductive cellular environments, limiting the application of in-cell DNP.[20,21] Although strategies have been proposed to circumvent this problem with in-cell DNP[21,22] and highly reactive surfaces,[23−25] the availability of alternative polarizing agents that are stable under such harsh conditions would facilitate more widespread application of MAS DNP.

Metal-based polarization agents could be good alternatives,[5] and some work has been reported on DNP from Cr(III),[26] Mn(II),[27] and V(IV).[28] In this class, Gd(III) complexes are the most promising alternatives due to the intrinsic chemical stability of the Gd(III) centers.[29] Gd(III) complexes also possess favorable EPR properties such as a quenched spin−orbit coupling and weak hyperfine couplings with $^{155/157}$Gd, in comparison to other paramagnetic metal ions.[30] Endogenous Gd(III) dopants have been used to hyperpolarize nuclei in inorganic solids such as metal oxides,[31,32] glasses,[33] and battery electrode materials;[34−36] for example, recently, Gd(III) has been shown to provide large ^{17}O solid effect DNP enhancements of 652 at 100 K and 320 at room temperature in ^{17}O-

Received: March 11, 2022
Revised: June 20, 2022
Published: July 5, 2022

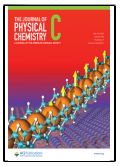

enriched ceria.[32] These high enhancements were attributed to the cubic environment of the metal in the ceria lattice and to the relatively small magnitude of the higher-order electrostatic multipoles, that in turn lead to relatively narrow EPR linewidths which can be easily saturated under DNP conditions. On the other hand, Griffin and co-workers demonstrated that the molecular Gd complexes $[Gd(dota)(H_2O)]^-$ and $[Gd(dtpa)(H_2O)]^{2-}$, hereafter abbreviated as Gd(dota) and Gd(dtpa), respectively (Figure 1A), could be used as exogenous polarizing agents in MAS DNP,[27] where Gd(dota) exhibited a relatively good solid effect ^{1}H DNP enhancement.[30] Bisgadolinium complexes have also been used for solid and cross effect DNP; however, relatively low ^{1}H DNP enhancements of around 4 were observed so far.[37] Recently, our group demonstrated a factor of two gain in DNP enhancement with Gd(tpatcn) in comparison to Gd(dota) (Figure 1A), which was ascribed to its lower mean zero-field splitting (ZFS).[38]

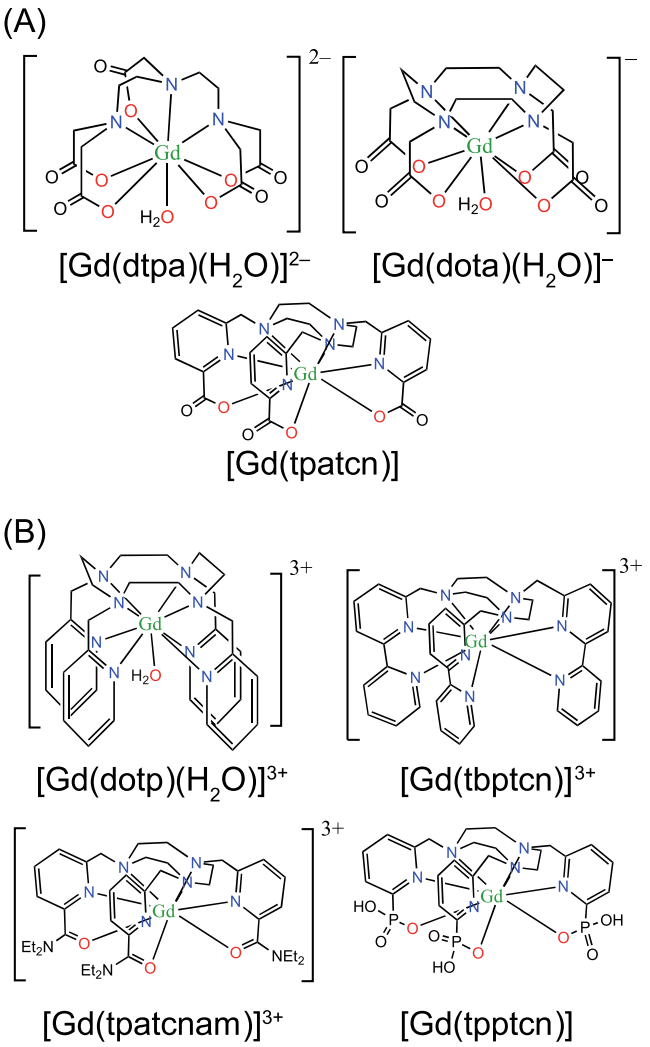

Figure 1. Chemical structures of (A) previously studied Gd complexes Gd(dtpa), Gd(dota), and Gd(tpatcn) and (B) Gd complexes studied in this work namely Gd(dotp), Gd(tbptcn), Gd(tpatcnam), and Gd(tpptcn). The directly coordinated oxygen atoms and nitrogen atoms are highlighted in red and blue, respectively. The positive and negative charges are balanced by I^- and Na^+ counterions, respectively.

Although Gd(dota) and Gd(tpatcn) as state-of-the-art Gd(III) polarizing agents have been used to perform DNP in biomolecular systems[30,39] or frozen aqueous solutions,[38] the observed DNP enhancements are still moderate when compared to efficient mononitroxide radicals.[17] Therefore, it is important to understand how to design Gd(III) polarizing agents to yield better DNP efficiency. In particular, we have proposed that high symmetry at the metal center can lead to lower ZFS, which will in turn provide better DNP efficiency.[38]

Here, we report DNP enhancements at 9.4 T for four Gd(III) complexes in aqueous solutions that have not previously been used for DNP, namely $[Gd(dotp)(H_2O)]^{3+}$, $[Gd(tbptcn)]^{3+}$, $[Gd(tpatcnam)]^{3+}$, and [Gd(tpptcn)] [denoted hereafter as Gd(dotp), Gd(tbptcn), Gd(tpatcnam), and Gd(tpptcn), respectively, Figure 1B]. We establish the reciprocal quadratic dependence of the ^{1}H DNP enhancement on the mean ZFS parameter D and the feasibility of designing Gd(III) polarizing agents by tuning ligand structures.

RESULTS AND DISCUSSION

Figure 1 shows the structures of the Gd complexes that were previously reported and those that are studied in this work. The corresponding measured DNP enhancements and EPR properties are provided in Table 1. Gd(dtpa) and Gd(dota) are both commercial magnetic resonance imaging contrast agents that contain octadentate chelating ligands and vacant coordination sites for solvent molecules.[29,40] With Gd(dota), we have previously observed a ^{1}H DNP enhancement of −17 at 9.4 T and 100 K in the standard water-based DNP glass-forming matrix glycerol-d_8/D_2O/H_2O (6:3:1).[38] However, Gd(dtpa) which has a much higher D value of 1568 MHz in comparison to 599 MHz for Gd(dota), showed a lower DNP enhancement of −3.6 (Table 1).[38] As mentioned above, the molecular Gd(III) complex that currently provides the highest ^{1}H DNP enhancement is Gd(tpatcn),[41] a nonadentate chelating complex that has a relatively narrow EPR spectrum (D = 400 MHz) and generates a ^{1}H DNP enhancement of −37,[38] which is comparable to current state-of-the-art monoradicals[17] and is, for example, significantly higher than the enhancement obtained with TEMPO at 9.4 T.

The three established Gd(III) complexes are stable in glycerol−water solutions and exist in well-defined structures (Figure 1A),[41−43] which are prerequisites for exploring the impact of the local structure and symmetry at the Gd metal center on the DNP efficiency. The complexes contain octa- or nonadentate chelating ligands, which are known to confer higher structural rigidity and stability in solution in the presence of coordinating solvents such as water.[29,44] Because such chelates are likely to also be more rigid in frozen solution, their structures should positively impact DNP performance.[45,46] Figure 1B shows the structures of the four new polarizing agents studied here that also contain 1:1 chelating octadentate or nonadentate ligands. Gd(dotp) and Gd(tbptcn) are cationic analogues of Gd(dota) and Gd(tpatcn), respectively,[47,48] where the carboxylate groups are replaced by 2-pyridyl groups to assess the impact of changes in the electronic charge distribution with nitrogen donors on the Gd ZFS and DNP enhancements. To specifically evaluate differences in basicity of the oxygen donor atoms of Gd(tpatcn), we synthesized Gd(tpatcnam), in which the carboxylate groups are replaced by diethylamide groups. Gd(tpptcn) was made by adapting the procedure reported for analogous lanthanide complexes to probe the importance of

https://doi.org/10.1021/acs.jpcc.2c01721
J. Phys. Chem. C 2022, 126, 11310−11317

Table 1. 9.4 T MAS ^{1}H DNP Parameters and Q-Band EPR Relaxation and ZFS Parameters

species	D (MHz)[a]	σ_D (MHz)	T_B (s)	T_{1e} (μs)	T_{2e} (μs)	T_{1e}·T_{2e} (μs^2)	^{1}H enhancement (ε)	contribution factor (θ)[d]	absolute sensitivity enhancement (Σ)[d]
Gd(dtpa)[b]	1568	728	15.7				−3.6	0.34	2.8
Gd(dota)[a]	599 ± 94	330 ± 214	12.8	0.7	0.3	0.21	−15.8	0.28	11.2
Gd(tpatcn)[a]	410 ± 25	106 ± 62	14.5	0.7	0.3	0.21	−35.5	0.38	32.1
Gd(dotp)[c]	1000 ± 100	250 ± 100	9.4	0.50	0.47	0.23	−6.8	0.40	8.0
Gd(tbptcn)	1125 ± 105	290 ± 80	12.8	0.86	0.46	0.40	−12.8	0.44	14.3
Gd(tpatcnam)	700 ± 75	233 ± 35	8.8	0.65	0.32	0.21	−12.9	0.32	12.6
Gd(tpptcn)	750 ± 40	224 ± 40	11.7	0.76	0.39	0.30	−17.3	0.41	19.6

[a]The DNP and EPR data of Gd(dota) and Gd(tpatcn) were taken from ref 38, which were obtained from experiments under corresponding conditions. [b]The ZFS parameters of Gd(dtpa) were taken from ref 30. [c]The EPR spectrum of Gd(dotp) was deconvoluted to two sites, with relative contributions of 85% ($D \sim 5000 \pm 500$ MHz, $\sigma_D = 300 \pm 120$ MHz) and 15% ($D \sim 1000 \pm 100$ MHz, $\sigma_D = 250 \pm 100$ MHz). Only the EPR properties of the low ZFS site are provided in the table, as this site will primarily contribute to the observed DNP enhancement. [d]The absolute sensitivity enhancement (Σ) is calculated using the equation $\Sigma = \epsilon\theta\sqrt{\frac{T_{Solvent}}{T_B}}$ with $T_{solvent} = 82$ s. The contribution factor (θ) is the ratio of the normalized, quantitative signal intensities of the solvent with and without the polarizing agent (see the Supporting Information).

high electronic density on donor atoms by introducing phosphate groups that have more delocalized negative charge than carboxylate groups.[49,50] The stability and structure of these complexes in water were confirmed from solution ^{1}H NMR of the corresponding Eu(III) analogues (Figures S3 and S4). Notably, for the complexes with three positive charges of Gd(III), the residual charge facilitates the solvation by water molecules such that the complexes with +3 charge dissolve more rapidly in an aqueous solution. Regardless of the kinetic factors, all of these complexes exhibit high solubilities, in the tens of millimolar regime, sufficient for DNP experiments. The very detailed structure of the solvation sphere in the frozen solutions may well cause slight distortions in the coordination geometry and be one of the contributing factors to the differences observed in the ZFS.

To study the impact of the structure of the Gd complexes on the ZFS and ultimately the DNP enhancements, we have carefully examined the relative differences in their crystal structures. The crystal structure of Gd(dotp), which was previously reported,[48] exhibits a monocapped square antiprism structure [similar to Gd(dota)]. Here, we obtained the crystal structures of the three other Gd complexes, i.e., Gd(tbptcn), Gd(tpatcnam), and Gd(tpptcn). According to the XRD results, the core coordination structure for Gd(tbptcn), Gd(tpatcnam) and Gd(tpptcn) can be described as a distorted tricapped trigonal prism with a pseudo-C_3 symmetry [analogous to Gd(tpatcn)] (Figure 2). The lower trigonal face that incorporates the three aliphatic nitrogen atoms from the 1,4,7-triazacyclononane moiety and the three pyridyl nitrogen atoms at the capping positions in Gd(tpatcn) are also present in the newly obtained structures (Figures 2, S5 and S6). The average N−Gd−N bond angles and Gd−N bond lengths in the lower trigonal face and the capping positions are similar to those of Gd(tpatcn) in all structures (Tables S2 and S3) due to the chemical similarity. The distance from the centroid of the atoms in the upper trigonal face to Gd shows that Gd(tpptcn) (1.476 Å) and Gd(tpatcnam) (1.533 Å) are similar to Gd(tpatcn) (1.489 Å), while they are all significantly different from Gd(tbptcn) (1.730 Å) due to the presence of nitrogen donors instead of oxygen (Table S5), in good agreement with the corresponding O-Gd−O and N−Gd−N bond angles (Table S3).

To evaluate the distortion from an ideal prism, we measured the angle made by the centroids of the two trigonal faces and

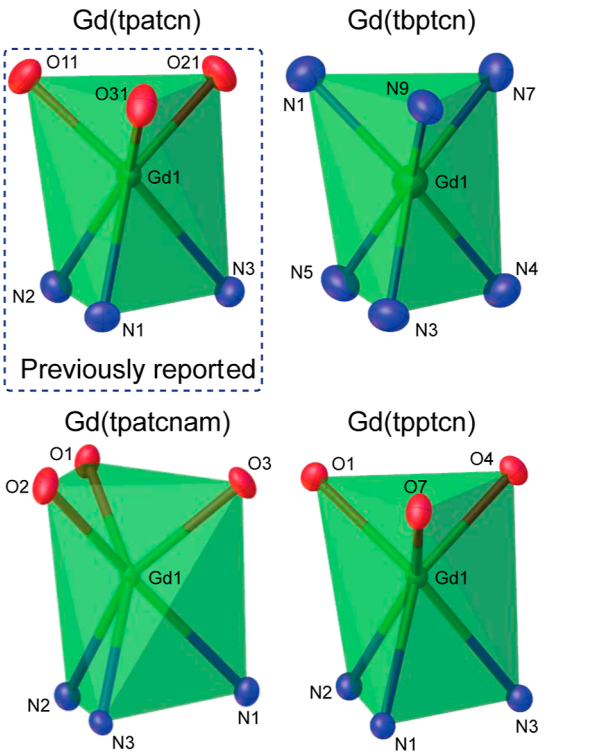

Figure 2. Comparison of the coordination geometry of the newly reported crystal structures with that of Gd(tpatcn). The donor atoms at capping positions are omitted.

the Gd center, which will be 180° for an ideal prism. Notably, for Gd(tpatcn) this angle is 179.80° with a deviation of only 0.20°, whereas the deviation is slightly larger in Gd(tbptcn) (0.84°), Gd(tpatcnam) (1.07°), and Gd(tpptcn) (0.83°), which may give rise to a larger ZFS. Another parameter that evaluates the distortion from an ideal prism is the average value of the torsion angles formed by the atoms of the rectangular faces which is found to be 19(2)° for Gd(tpptcn) and 22.1(7)° for Gd(tbptcn), which are similar as compared to Gd(tpatcn) [21.8(7)°], but which is found to be −24(3)° for Gd(tpatcnam). These similar absolute values for all the torsion angles cause similarity in the difference in orientation between two trigonal faces among these four complexes, but with Gd(tpatcnam) being twisted in the opposite direction (Figure

https://doi.org/10.1021/acs.jpcc.2c01721
J. Phys. Chem. C 2022, 126, 11310−11317

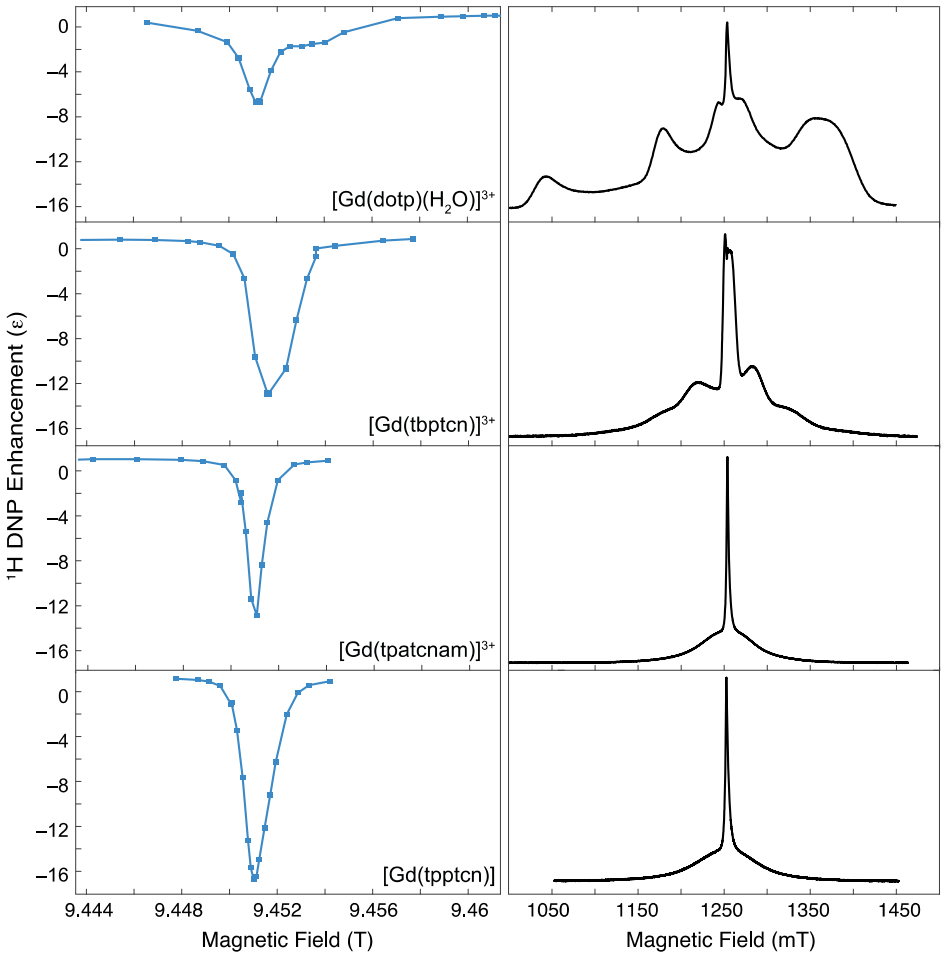

Figure 3. (Left) ^{1}H MAS DNP Zeeman field profiles and (right) Q band echo-detected EPR field sweep spectra of (top to bottom) Gd(dotp), Gd(tbptcn), Gd(tpatcnam), and Gd(tpptcn) in glycerol-d_8/D_2O/H_2O (6:3:1). MAS DNP experiments were performed at 100 K with 4 mM solutions, and the EPR experiments were performed at 10 K with 25 μM solutions.

S6). The distortion we discuss here is in crystals, therefore it could be related to intermolecular interactions, which are negligible in a dilute aqueous solution. Nevertheless, the fact that the distortion from an ideal prism is the lowest for Gd(tpatcn) is probably why it also has the lowest ZFS.[51] Indeed, a similar twist angle has been linked to lower ZFS in six-coordinated Mn(II) complexes.[52]

Figure 3 shows the negative lobe of the ^{1}H DNP Zeeman field profiles for MAS DNP experiments at 9.4 T of 4 mM solutions of the new complexes in glycerol-d_8/D_2O/H_2O (6:3:1) solutions. A fixed concentration (4 mM) was chosen here as this was found to be optimal previously.[38] The DNP enhancement was measured by taking the ratio of the integrated signal intensities of the direct 1D ^{1}H or ^{1}H → ^{13}C CP spectra with and without microwave irradiation. Despite the differences in absolute enhancements, the profiles resemble the typical shape of the solid effect, where a symmetric negative peak appears at a frequency that is one ^{1}H Larmor frequency higher than the electronic Larmor frequency. Among the four new complexes, Gd(tpptcn) is the most efficient polarizing agent and provides a DNP enhancement of −17.3, which is comparable to Gd(dota), while the other two nonadentate complexes Gd(tpatcnam) and Gd(tbptcn) show slightly lower enhancements of −13. Combined with the similarity between Gd(tpptcn) and Gd(tpatcn) observed in the crystal structures, the relatively high enhancement of Gd(tpptcn) is expected. Considering the weaker basicity of the phosphate acid group than the carboxylate group, the high electron density on the donor atom could benefit DNP performance in Gd(III) complexes. Gd(dotp), the structural analogue of Gd(dota) that has a coordination vacancy for solvent molecules, showed the lowest enhancement of −6.8, which is still higher than that of Gd(dtpa). The maximum negative DNP enhancements were all observed within a range smaller than 100 ppm.

Mono-Gd(III) complexes exhibit DNP mainly via the solid effect between the nuclear spin and the central transition of Gd (m_s = −1/2 to +1/2) because the central transition is broadened by ZFS only to the second order, which scales proportionally to D^2/ω_{0S}, whereas the satellite transitions are severely broadened by the first-order ZFS interaction which makes solid effect inefficient. Here, D is the axial component of ZFS which can be extracted from the EPR spectra. Therefore, neglecting other broadening factors, the maximum enhancement of a series of Gd(III) polarizing agents is predicted to be inversely proportional to the square of D (eq 1),[38] which was compatible with the enhancements observed for Gd(dota) and Gd(tpatcn). A detailed theoretical appendix can be found in the Supporting Information of the work by Stevanato et al.[38]

https://doi.org/10.1021/acs.jpcc.2c01721
J. Phys. Chem. C 2022, 126, 11310−11317

$$\frac{\varepsilon_1}{\varepsilon_2} \approx \left(\frac{D_2}{D_1}\right)^2 \quad (1)$$

To measure D of the Gd complexes, we performed Q-band echo detected EPR experiments (Figure 3). The spectra were recorded at 10 K in 25 μM frozen solutions to remove any relaxation bias of the signal intensities of the different transitions and reduce Gd spin−spin interactions. Table 1 shows the mean ZFS D value and σ_D, the width of the distribution of D, which were extracted by fitting the EPR spectra (details in the Supporting Information). Gd(tpptcn) and Gd(tpatcnam) show field sweep EPR spectra composed of one narrow peak corresponding to the central transition and broad shoulder peaks corresponding to the satellite transitions, which are typical for weak-ZFS complexes as observed previously.[27,38] Therefore, we used model 2 reported by Clayton et al.[51,53] for Gd(tpptcn) and Gd(tpatcnam) which includes a Gaussian distribution for D and a random distribution for E/D that is limited to 0−1/3, by definition. With this method, we measured D values of 700 and 750 MHz for Gd(tpatcnam) and Gd(tpptcn), which are higher than those of both Gd(dota) and Gd(tpatcn). For Gd(tbptcn), we used model 1 to include a separate distribution for E and determined the D value of Gd(tbptcn) to be 1125 MHz. In the case of Gd(dotp), we observed two components in the EPR spectrum (D of ca. 1000 MHz and 5000 MHz for the narrow and broad components, respectively), and the component with smaller D is likely to make the only significant contribution to the DNP enhancement. The presence of two components in the EPR spectrum and the relatively low DNP enhancement with Gd(dotp) might be attributed to the isomerization in the aqueous solution which has been observed for the Eu(III) analogue.[48]

Besides ZFS, another crucial parameter that affects the saturation of the EPR transitions and DNP is the relaxation of the electron spins, which is characterized by the longitudinal (T_1) and transverse (T_2) relaxation times. Long electronic relaxation times will improve the saturation of the electronic transitions under the continuous-wave microwave irradiation and will enable efficient DNP at lower microwave powers. This is particularly important for solid effect DNP because forbidden double quantum or zero quantum transitions are saturated, which require higher microwave powers. Previously, similar electron relaxation times (T_{1e} = 0.7 μs and T_{2e} = 0.3 μs) were observed with both Gd(tpatcn) and Gd(dota) at 100 K.[27,38] Here, we find that under the same conditions, the T_{1e} and T_{2e} relaxation times of all the complexes fall within similar ranges of 0.5−0.8 and 0.3−0.5 μs, respectively, with Gd(tbptcn) and Gd(tpptcn) showing slightly longer relaxation times than the rest of the complexes (Table 1). These values are characteristics of relaxation time distributions, whose width and shape are characterized by stretch exponents of 0.7−0.85 for T_{1e} and 1.2−1.5 for T_{2e} (Figure S10). Note that a large fraction of the electron spins relaxes faster than the detection limit of echo-detected EPR spectroscopy at 100 K, resulting in measured relaxation times that represent only a fraction of the entire distribution. However, the portion neglected by EPR will also contribute less to DNP at 100 K, therefore measuring relaxation times via pulsed EPR spectroscopy is still an effective method to qualitatively characterize the relaxation properties of DNP polarizing agents. Although fluctuations in ZFS are expected to be the primary mechanism for electronic transverse relaxation in Gd(III) in frozen solutions at 100 K, T_{2e} of the central transition is also affected by nuclear spin diffusion.[54] On the other hand, the Gd(III) electron T_1 relaxation is expected to be caused by fluctuations of the orbit−lattice coupling.[55] The observed electron relaxation times are largely similar within the series here (Table 1), and the relative differences inside the series are likely caused by differing electron−proton interactions, as for example partially deuterated solvents have shown to provide longer electronic transverse relaxation times.[55] Given that the EPR relaxation times were measured in the same solvent mixture for all samples in this work (glycerol-d_8/D_2O/H_2O (6:3:1 by volume)), and that the relaxation times are largely similar, it is clear that differences in electron relaxation and ZFS are not strongly correlated in these compounds. The similarity of the relaxation values and stretch exponents also indicates that the DNP enhancements are likely limited by saturation of the broad, inhomogeneous central transition signals primarily due to differences in the ZFS. Note that the saturation level achieved is likely only a few % given that the microwave B_1 fields are estimated to be a few hundred kHz,[56] whereas the central transition EPR linewidths are approximately 5−15 MHz at 9.4 T.

Finally, in Figure 4 we compare the measured D and ^{1}H DNP enhancements for all the mononuclear Gd complexes

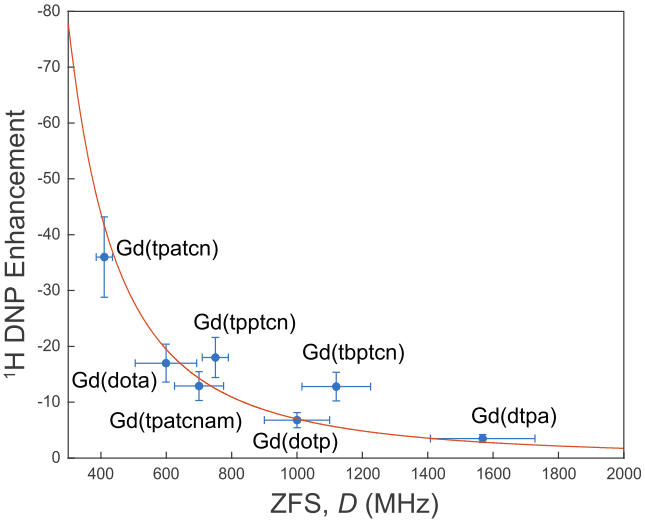

Figure 4. Plot showing the correlation between measured ^{1}H DNP enhancement and the measured ZFS parameter D. The red curve is a fit to a reciprocal quadratic relationship (eq 1). Error bars on the enhancements are estimated to be 20%.

hitherto reported, to evaluate the impact of ZFS on DNP. The figure illustrates a strong reciprocal quadratic relationship between D and ^{1}H DNP, confirming that this simple relationship can be used to predict the DNP performance of Gd(III) polarizing agents. Among the seven complexes, only Gd(tbptcn) and Gd(tpptcn) are significantly above the curve, and the deviation can be explained by their relatively large mean saturation factors of 0.40 and 0.30 μs^2 in comparison to the other complexes, which show 0.21−0.23 μs^2 (Table 1). Consequently, in these two cases the Gd central transition is better saturated, and slightly higher DNP enhancements are observed. Nevertheless, it is clear that unless the saturation factor can be significantly improved (>1 μs^2), the ZFS is the dominant parameter that limits DNP enhancements. Although

https://doi.org/10.1021/acs.jpcc.2c01721
J. Phys. Chem. C 2022, 126, 11310−11317

Gd(tpatcn) remains the most efficient Gd(III) polarizing agent, the establishment of the correlation between ZFS and DNP enhancement is useful as it supports the possibility to screen Gd(III)-based polarizing agents based on their chemical structure.

CONCLUSIONS

In this work, we have introduced four Gd(III) chelate complexes to explore the relationship between the ZFS D and DNP performance. On comparing the ^{1}H MAS DNP enhancement measured at 9.4 T and the electronic properties extracted from the Q-band EPR spectra, we observed that the main factor explaining DNP performance is an inverse quadratic dependence between the DNP enhancement and the ZFS parameter D, in very good agreement with theory. This is due to the limited microwave saturation of the Gd(III) EPR central transitions when ZFS is higher. We also see some evidence that the electronic relaxation times then make a smaller but noticeable contribution, again in good agreement with expectations from theory. Finally, we noted that the distortion from an ideal prism is likely an important structural parameter that could be linked to ZFS. Although none of the complexes yield a higher DNP enhancement than Gd(tpatcn), the relationship established here will notably enable the search for improved Gd(III) polarizing agents in the future.

ASSOCIATED CONTENT

Supporting Information

The Supporting Information is available free of charge at https://pubs.acs.org/doi/10.1021/acs.jpcc.2c01721.

Experimental details, spectral assignment, fitting details and a link to all the raw EPR and NMR data (https://doi.org/10.5281/zenodo.6787801), and MATLAB codes (PDF)

Accession Codes

Crystal structures of Gd(tbptcn), Gd(tpatcnam), and Gd(tpptcn) are made available in the Cambridge structural database (CSD codes: 2157517, 2157502, and 2157518).

AUTHOR INFORMATION

Corresponding Author

Lyndon Emsley − *Laboratory of Magnetic Resonance, Institut des Sciences et Ingénierie Chimiques, École Polytechnique Fédérale de Lausanne (EPFL), CH-1015 Lausanne, Switzerland;* orcid.org/0000-0003-1360-2572; Email: lyndon.emsley@epfl.ch

Authors

Yu Rao − *Laboratory of Magnetic Resonance, Institut des Sciences et Ingénierie Chimiques, École Polytechnique Fédérale de Lausanne (EPFL), CH-1015 Lausanne, Switzerland;* orcid.org/0000-0002-9787-5596

Chad T. Palumbo − *Group of Coordination Chemistry, Institut des Sciences et Ingénierie Chimiques, École Polytechnique Fédérale de Lausanne (EPFL, CH-1015 Lausanne, Switzerland*

Amrit Venkatesh − *Laboratory of Magnetic Resonance, Institut des Sciences et Ingénierie Chimiques, École Polytechnique Fédérale de Lausanne (EPFL), CH-1015 Lausanne, Switzerland;* orcid.org/0000-0001-5319-9269

Megan Keener − *Group of Coordination Chemistry, Institut des Sciences et Ingénierie Chimiques, École Polytechnique Fédérale de Lausanne (EPFL, CH-1015 Lausanne, Switzerland*

Gabriele Stevanato − *Laboratory of Magnetic Resonance, Institut des Sciences et Ingénierie Chimiques, École Polytechnique Fédérale de Lausanne (EPFL), CH-1015 Lausanne, Switzerland;* orcid.org/0000-0003-0020-1286

Anne-Sophie Chauvin − *Group of Coordination Chemistry, Institut des Sciences et Ingénierie Chimiques, École Polytechnique Fédérale de Lausanne (EPFL, CH-1015 Lausanne, Switzerland;* orcid.org/0000-0001-9222-3866

Georges Menzildjian − *Laboratory of Magnetic Resonance, Institut des Sciences et Ingénierie Chimiques, École Polytechnique Fédérale de Lausanne (EPFL), CH-1015 Lausanne, Switzerland;* orcid.org/0000-0001-6285-0447

Sergei Kuzin − *Laboratory of Physical Chemistry, Department of Chemistry, ETH Zürich, CH-8093 Zürich, Switzerland*

Maxim Yulikov − *Laboratory of Physical Chemistry, Department of Chemistry, ETH Zürich, CH-8093 Zürich, Switzerland;* orcid.org/0000-0003-3275-0714

Gunnar Jeschke − *Laboratory of Physical Chemistry, Department of Chemistry, ETH Zürich, CH-8093 Zürich, Switzerland;* orcid.org/0000-0001-6853-8585

Anne Lesage − *Centre de RMN à Très Hauts Champs, Université de Lyon (CNRS/ENS Lyon/UCB Lyon 1), 69100 Villeurbanne, France;* orcid.org/0000-0003-1958-2840

Marinella Mazzanti − *Group of Coordination Chemistry, Institut des Sciences et Ingénierie Chimiques, École Polytechnique Fédérale de Lausanne (EPFL, CH-1015 Lausanne, Switzerland;* orcid.org/0000-0002-3427-008X

Complete contact information is available at: https://pubs.acs.org/10.1021/acs.jpcc.2c01721

Author Contributions

The manuscript was written through contributions of all authors. All authors have given approval to the final version of the manuscript

Notes

The authors declare no competing financial interest.

ACKNOWLEDGMENTS

Financial support from Swiss National Science Foundation Grant no. 200020_178860 is acknowledged. A.V. acknowledges H2020 Marie Skłodowska-Curie Individual fellowship (grant number 101024369). The authors thank Luana Trovatelli and Lisa Rosselet, who contributed to the synthesis of tpatcnam and tpptcn ligands during their apprentice internship. We acknowledge Jessica Clayton and Katharina Keller for providing MATLAB codes which were modified to fit the Gd EPR spectra.

REFERENCES

(1) Hodgkinson, P. *Modern Methods in Solid-state NMR: A Practitioner's Guide*; Royal Society of Chemistry, 2018.

(2) Reif, B.; Ashbrook, S. E.; Emsley, L.; Hong, M. Solid-state NMR spectroscopy. *Nat. Rev. Methods Primers* **2021**, *1*, 2.

(3) Ni, Q. Z.; Daviso, E.; Can, T. V.; Markhasin, E.; Jawla, S. K.; Swager, T. M.; Temkin, R. J.; Herzfeld, J.; Griffin, R. G. High Frequency Dynamic Nuclear Polarization. *Acc. Chem. Res.* **2013**, *46*, 1933−1941.

(4) Rossini, A. J.; Zagdoun, A.; Lelli, M.; Lesage, A.; Copéret, C.; Emsley, L. Dynamic Nuclear Polarization Surface Enhanced NMR Spectroscopy. *Acc. Chem. Res.* **2013**, *46*, 1942−1951.

(5) Lilly Thankamony, A. S.; Wittmann, J. J.; Kaushik, M.; Corzilius, B. Dynamic Nuclear Polarization for Sensitivity Enhancement in Modern Solid-State NMR. *Prog. Nucl. Magn. Reson. Spectrosc.* **2017**, *102*−*103*, 120−195.
(6) Debelouchina, G. T.; Bayro, M. J.; van der Wel, P. C. A.; Caporini, M. A.; Barnes, A. B.; Rosay, M.; Maas, W. E.; Griffin, R. G. Dynamic Nuclear Polarization-Enhanced Solid-State NMR Spectroscopy of GNNQQNY Nanocrystals and Amyloid Fibrils. *Phys. Chem. Chem. Phys.* **2010**, *12*, 5911−5919.
(7) Kaplan, M.; Cukkemane, A.; van Zundert, G. C. P.; Narasimhan, S.; Daniëls, M.; Mance, D.; Waksman, G.; Bonvin, A. M. J. J.; Fronzes, R.; Folkers, G. E.; et al. Probing a Cell-Embedded Megadalton Protein Complex by DNP-Supported Solid-State NMR. *Nat. Methods* **2015**, *12*, 649−652.
(8) Gupta, R.; Lu, M.; Hou, G.; Caporini, M. A.; Rosay, M.; Maas, W.; Struppe, J.; Suiter, C.; Ahn, J.; Byeon, I.-J. L.; et al. Dynamic Nuclear Polarization Enhanced MAS NMR Spectroscopy for Structural Analysis of HIV-1 Protein Assemblies. *J. Phys. Chem. B* **2016**, *120*, 329−339.
(9) Piveteau, L.; Ong, T.-C.; Walder, B. J.; Dirin, D. N.; Moscheni, D.; Schneider, B.; Bär, J.; Protesescu, L.; Masciocchi, N.; Guagliardi, A.; et al. Resolving the Core and the Surface of CdSe Quantum Dots and Nanoplatelets Using Dynamic Nuclear Polarization Enhanced PASS-PIETA NMR Spectroscopy. *ACS Cent. Sci.* **2018**, *4*, 1113−1125.
(10) Narasimhan, S.; Scherpe, S.; Lucini Paioni, A.; van der Zwan, J.; Folkers, G. E.; Ovaa, H.; Baldus, M. DNP-Supported Solid-State NMR Spectroscopy of Proteins Inside Mammalian Cells. *Angew. Chem., Int. Ed.* **2019**, *58*, 12969−12973.
(11) Gauto, D.; Dakhlaoui, O.; Marin-Montesinos, I.; Hediger, S.; De Paëpe, G. Targeted DNP for biomolecular solid-state NMR. *Chem. Sci.* **2021**, *12*, 6223−6237.
(12) Perras, F. A.; Paterson, A. L.; Syed, Z. H.; Kropf, A. J.; Kaphan, D. M.; Delferro, M.; Pruski, M. Revealing the Configuration and Conformation of Surface Organometallic Catalysts with DNP-Enhanced NMR. *J. Phys. Chem. C* **2021**, *125*, 13433−13442.
(13) Zagdoun, A.; Casano, G.; Ouari, O.; Schwarzwälder, M.; Rossini, A. J.; Aussenac, F.; Yulikov, M.; Jeschke, G.; Copéret, C.; Lesage, A.; et al. Large Molecular Weight Nitroxide Biradicals Providing Efficient Dynamic Nuclear Polarization at Temperatures up to 200 K. *J. Am. Chem. Soc.* **2013**, *135*, 12790−12797.
(14) Sauvée, C.; Rosay, M.; Casano, G.; Aussenac, F.; Weber, R. T.; Ouari, O.; Tordo, P. Highly Efficient, Water-Soluble Polarizing Agents for Dynamic Nuclear Polarization at High Frequency. *Angew. Chem., Int. Ed.* **2013**, *125*, 11058−11061.
(15) Mentink-Vigier, F.; Marin-Montesinos, I.; Jagtap, A. P.; Halbritter, T.; van Tol, J.; Hediger, S.; Lee, D.; Sigurdsson, S. T.; De Paëpe, G. Computationally Assisted Design of Polarizing Agents for Dynamic Nuclear Polarization Enhanced NMR: The AsymPol Family. *J. Am. Chem. Soc.* **2018**, *140*, 11013−11019.
(16) Lund, A.; Casano, G.; Menzildjian, G.; Kaushik, M.; Stevanato, G.; Yulikov, M.; Jabbour, R.; Wisser, D.; Renom-Carrasco, M.; Thieuleux, C.; et al. TinyPols: a Family of Water-Soluble Binitroxides Tailored for Dynamic Nuclear Polarization Enhanced NMR Spectroscopy at 18.8 and 21.1 T. *Chem. Sci.* **2020**, *11*, 2810−2818.
(17) Stevanato, G.; Casano, G.; Kubicki, D. J.; Rao, Y.; Esteban Hofer, L.; Menzildjian, G.; Karoui, H.; Siri, D.; Cordova, M.; Yulikov, M.; et al. Open and Closed Radicals: Local Geometry around Unpaired Electrons Governs Magic-Angle Spinning Dynamic Nuclear Polarization Performance. *J. Am. Chem. Soc.* **2020**, *142*, 16587−16599.
(18) Mathies, G.; Caporini, M. A.; Michaelis, V. K.; Liu, Y.; Hu, K. N.; Mance, D.; Zweier, J. L.; Rosay, M.; Baldus, M.; Griffin, R. G. Efficient Dynamic Nuclear Polarization at 800 MHz/527 GHz with Trityl-Nitroxide Biradicals. *Angew. Chem., Int. Ed.* **2015**, *54*, 11770−11774.
(19) Wisser, D.; Karthikeyan, G.; Lund, A.; Casano, G.; Karoui, H.; Yulikov, M.; Menzildjian, G.; Pinon, A. C.; Purea, A.; Engelke, F.; et al. BDPA-Nitroxide Biradicals Tailored for Efficient Dynamic Nuclear Polarization Enhanced Solid-State NMR at Magnetic Fields up to 21.1 T. *J. Am. Chem. Soc.* **2018**, *140*, 13340−13349.
(20) Azarkh, M.; Okle, O.; Eyring, P.; Dietrich, D. R.; Drescher, M. Evaluation of Spin Labels for In-Cell EPR by Analysis of Nitroxide Reduction in Cell Extract of Xenopus Laevis Oocytes. *J. Magn. Reson.* **2011**, *212*, 450−454.
(21) Ghosh, R.; Xiao, Y.; Kragelj, J.; Frederick, K. K. In-Cell Sensitivity-Enhanced NMR of Intact Viable Mammalian Cells. *J. Am. Chem. Soc.* **2021**, *143*, 18454−18466.
(22) Albert, B. J.; Gao, C.; Sesti, E. L.; Saliba, E. P.; Alaniva, N.; Scott, F. J.; Sigurdsson, S. T.; Barnes, A. B. Dynamic Nuclear Polarization Nuclear Magnetic Resonance in Human Cells Using Fluorescent Polarizing Agents. *Biochemistry* **2018**, *57*, 4741−4746.
(23) Liao, W.-C.; Ong, T.-C.; Gajan, D.; Bernada, F.; Sauvée, C.; Yulikov, M.; Pucino, M.; Schowner, R.; Schwarzwälder, M.; Buchmeiser, M. R.; et al. Dendritic polarizing agents for DNP SENS. *Chem. Sci.* **2017**, *8*, 416−422.
(24) Pump, E.; Viger-Gravel, J.; Abou-Hamad, E.; Samantaray, M. K.; Hamzaoui, B.; Gurinov, A.; Anjum, D. H.; Gajan, D.; Lesage, A.; Bendjeriou-Sedjerari, A.; et al. Reactive Surface Organometallic Complexes Observed using Dynamic Nuclear Polarization Surface Enhanced NMR Spectroscopy. *Chem. Sci.* **2017**, *8*, 284−290.
(25) Yakimov, A. V.; Mance, D.; Searles, K.; Copéret, C. A Formulation Protocol with Pyridine to Enable Dynamic Nuclear Polarization Surface-Enhanced NMR Spectroscopy on Reactive Surface Sites: Case Study with Olefin Polymerization and Metathesis Catalysts. *J. Phys. Chem. Lett.* **2020**, *11*, 3401−3407.
(26) Abraham, M.; McCausland, M. A. H.; Robinson, F. N. H. Dynamic Nuclear Polarization. *Phys. Rev. Lett.* **1959**, *2*, 449−451.
(27) Corzilius, B.; Smith, A. A.; Barnes, A. B.; Luchinat, C.; Bertini, I.; Griffin, R. G. High-Field Dynamic Nuclear Polarization with High-Spin Transition Metal Ions. *J. Am. Chem. Soc.* **2011**, *133*, 5648−5651.
(28) Jain, S. K.; Yu, C.-J.; Wilson, C. B.; Tabassum, T.; Freedman, D. E.; Han, S. Dynamic Nuclear Polarization with Vanadium(IV) Metal Centers. *Chem* **2021**, *7*, 421−435.
(29) Caravan, P.; Ellison, J. J.; McMurry, T. J.; Lauffer, R. B. Gadolinium(III) Chelates as MRI Contrast Agents: Structure, Dynamics, and Applications. *Chem. Rev.* **1999**, *99*, 2293−2352.
(30) Kaushik, M.; Bahrenberg, T.; Can, T. V.; Caporini, M. A.; Silvers, R.; Heiliger, J.; Smith, A. A.; Schwalbe, H.; Griffin, R. G.; Corzilius, B. Gd(III) and Mn(II) Complexes for Dynamic Nuclear Polarization: Small Molecular Chelate Polarizing Agents and Applications with Site-Directed Spin Labeling of Proteins. *Phys. Chem. Chem. Phys.* **2016**, *18*, 27205−27218.
(31) Hope, M. A.; Björgvinsdóttir, S.; Grey, C. P.; Emsley, L. A Magic Angle Spinning Activated ^{17}O DNP Raser. *J. Phys. Chem. Lett.* **2021**, *12*, 345−349.
(32) Hope, M. A.; Björgvinsdóttir, S.; Halat, D. M.; Menzildjian, G.; Wang, Z.; Zhang, B.; MacManus-Driscoll, J. L.; Lesage, A.; Lelli, M.; Emsley, L.; et al. Endogenous ^{17}O Dynamic Nuclear Polarization of Gd-Doped CeO_2 from 100 to 370 K. *J. Phys. Chem. C* **2021**, *125*, 18799−18809.
(33) Paterson, A. L.; Perras, F. A.; Besser, M. F.; Pruski, M. Dynamic Nuclear Polarization of Metal-Doped Oxide Glasses: A Test of the Generality of Paramagnetic Metal Polarizing Agents. *J. Phys. Chem. C* **2020**, *124*, 23126−23133.
(34) Wolf, T.; Kumar, S.; Singh, H.; Chakrabarty, T.; Aussenac, F.; Frenkel, A. I.; Major, D. T.; Leskes, M. Endogenous Dynamic Nuclear Polarization for Natural Abundance ^{17}O and Lithium NMR in the Bulk of Inorganic Solids. *J. Am. Chem. Soc.* **2019**, *141*, 451−462.
(35) Jardón-Álvarez, D.; Reuveni, G.; Harchol, A.; Leskes, M. Enabling Natural Abundance ^{17}O Solid-State NMR by Direct Polarization from Paramagnetic Metal Ions. *J. Phys. Chem. Lett.* **2020**, *11*, 5439−5445.
(36) Haber, S.; Rosy; Saha, A.; Brontvein, O.; Carmieli, R.; Zohar, A.; Noked, M.; Leskes, M. Structure and Functionality of an Alkylated $Li_xSi_yO_z$ Interphase for High-Energy Cathodes from DNP-ssNMR Spectroscopy. *J. Am. Chem. Soc.* **2021**, *143*, 4694−4704.

(37) Kaushik, M.; Qi, M.; Godt, A.; Corzilius, B. Bis-Gadolinium Complexes for Solid Effect and Cross Effect Dynamic Nuclear Polarization. *Angew. Chem., Int. Ed.* **2017**, *56*, 4295−4299.
(38) Stevanato, G.; Kubicki, D. J.; Menzildjian, G.; Chauvin, A.-S.; Keller, K.; Yulikov, M.; Jeschke, G.; Mazzanti, M.; Emsley, L. A Factor Two Improvement in High-Field Dynamic Nuclear Polarization from Gd(III) Complexes by Design. *J. Am. Chem. Soc.* **2019**, *141*, 8746−8751.
(39) Heiliger, J.; Matzel, T.; Çetiner, E. C.; Schwalbe, H.; Kuenze, G.; Corzilius, B. Site-specific dynamic nuclear polarization in a Gd(III)-labeled protein. *Phys. Chem. Chem. Phys.* **2020**, *22*, 25455−25466.
(40) Wahsner, J.; Gale, E. M.; Rodríguez-Rodríguez, A.; Caravan, P. Chemistry of MRI Contrast Agents: Current Challenges and New Frontiers. *Chem. Rev.* **2019**, *119*, 957−1057.
(41) Gateau, C.; Mazzanti, M.; Pécaut, J.; Dunand, F. A.; Helm, L. Solid-State and Solution Properties of the Lanthanide Complexes of a New Nonadentate Tripodal Ligand derived from 1,4,7-Triazacyclononane. *Dalton Trans.* **2003**, 2428−2433.
(42) Chang, C. A.; Francesconi, L. C.; Malley, M. F.; Kumar, K.; Gougoutas, J. Z.; Tweedle, M. F.; Lee, D. W.; Wilson, L. J. Synthesis, Characterization, and Crystal-Structures of M(DO3A) (M = Fe, Gd) and Na[M(Dota)] (M = Fe, Y, Gd). *Inorg. Chem.* **1993**, *32*, 3501−3508.
(43) Zhao, B.; Chen, X.-Y.; Wang, W.-Z.; Cheng, P.; Ding, B.; Liao, D.-Z.; Yan, S.-P.; Jiang, Z.-H. $\{[GdAg_2(dtpa)(H_2O)]$center $3H_2O\}_n$: the First 2D Gd-Ag Coordination Polymer with Ag-Ag interaction. *Inorg. Chem. Commun.* **2005**, *8*, 178−181.
(44) Merbach, A. S.; Helm, L.; Toth, E. *The chemistry of contrast agents in medical magnetic resonance imaging*; John Wiley & Sons, 2013.
(45) Zagdoun, A.; Casano, G.; Ouari, O.; Lapadula, G.; Rossini, A. J.; Lelli, M.; Baffert, M.; Gajan, D.; Veyre, L.; Maas, W. E.; et al. A Slowly Relaxing Rigid Biradical for Efficient Dynamic Nuclear Polarization Surface-Enhanced NMR Spectroscopy: Expeditious Characterization of Functional Group Manipulation in Hybrid Materials. *J. Am. Chem. Soc.* **2012**, *134*, 2284−2291.
(46) Ong, T.-C.; Mak-Jurkauskas, M. L.; Walish, J. J.; Michaelis, V. K.; Corzilius, B.; Smith, A. A.; Clausen, A. M.; Cheetham, J. C.; Swager, T. M.; Griffin, R. G. Solvent-Free Dynamic Nuclear Polarization of Amorphous and Crystalline ortho-Terphenyl. *J. Phys. Chem. B* **2013**, *117*, 3040−3046.
(47) Prodi, L.; Maestri, M.; Ziessel, R.; Balzani, V. Luminescent Eu^{3+}, Tb^{3+}, and Gd^{3+} Complexes of a Branched-Triazacyclononane Ligand Containing 3 2,2'-Bipyridine Units. *Inorg. Chem.* **1991**, *30*, 3798−3802.
(48) Natrajan, L. S.; Khoabane, N. M.; Dadds, B. L.; Muryn, C. A.; Pritchard, R. G.; Heath, S. L.; Kenwright, A. M.; Kuprov, I.; Faulkner, S. Probing the Structure, Conformation, and Stereochemical Exchange in a Family of Lanthanide Complexes derived from Tetrapyridyl-appended Cyclen. *Inorg. Chem.* **2010**, *49*, 7700−7709.
(49) Nocton, G. g.; Nonat, A.; Gateau, C.; Mazzanti, M. Water Stability and Luminescence of Lanthanide Complexes of Tripodal Ligands Derived from 1,4,7-Triazacyclononane: Pyridinecarboxamide versus Pyridinecarboxylate Donors. *Helv. Chim. Acta* **2009**, *92*, 2257−2273.
(50) Salaam, J.; Tabti, L.; Bahamyirou, S.; Lecointre, A.; Hernandez Alba, O.; Jeannin, O.; Camerel, F.; Cianférani, S.; Bentouhami, E.; Nonat, A. M.; et al. Formation of Mono- and Polynuclear Luminescent Lanthanide Complexes based on the Coordination of Preorganized Phosphonated Pyridines. *Inorg. Chem.* **2018**, *57*, 6095−6106.
(51) Clayton, J. A.; Keller, K.; Qi, M.; Wegner, J.; Koch, V.; Hintz, H.; Godt, A.; Han, S.; Jeschke, G.; Sherwin, M. S.; et al. Quantitative analysis of zero-field splitting parameter distributions in Gd(iii) complexes. *Phys. Chem. Chem. Phys.* **2018**, *20*, 10470−10492.
(52) Uzal-Varela, R.; Valencia, L.; Lalli, D.; Maneiro, M.; Esteban-Gómez, D.; Platas-Iglesias, C.; Botta, M.; Rodríguez-Rodríguez, A. Understanding the Effect of the Electron Spin Relaxation on the Relaxivities of Mn(II) Complexes with Triazacyclononane Derivatives. *Inorg. Chem.* **2021**, *60*, 15055−15068.
(53) Raitsimring, A. M.; Astashkin, A. V.; Poluektov, O. G.; Caravan, P. High-Field Pulsed EPR and ENDOR of Gd^{3+} Complexes in Glassy Solutions. *Appl. Magn. Reson.* **2005**, *28*, 281−295.
(54) Raitsimring, A.; Dalaloyan, A.; Collauto, A.; Feintuch, A.; Meade, T.; Goldfarb, D. Zero Field Splitting Fluctuations Induced Phase Relaxation of Gd^{3+} in Frozen Solutions at Cryogenic Temperatures. *J. Magn. Reson.* **2014**, *248*, 71−80.
(55) Garbuio, L.; Zimmermann, K.; Häussinger, D.; Yulikov, M. Gd(III) Complexes for Electron-Electron Dipolar Spectroscopy: Effects of Deuteration, pH and Zero Field Splitting. *J. Magn. Reson.* **2015**, *259*, 163−173.
(56) Kubicki, D. J.; Rossini, A. J.; Purea, A.; Zagdoun, A.; Ouari, O.; Tordo, P.; Engelke, F.; Lesage, A.; Emsley, L. Amplifying Dynamic Nuclear Polarization of Frozen Solutions by Incorporating Dielectric Particles. *J. Am. Chem. Soc.* **2014**, *136*, 15711−15718.

https://doi.org/10.1021/acs.jpcc.2c01721
J. Phys. Chem. C 2022, 126, 11310−11317